PHYSICAL REVIEW D

PARTICLES, FIELDS, GRAVITATION, AND COSMOLOGY

THIRD SERIES, VOLUME 54, NUMBER 4 15 AUGUST 1996

ARTICLES

Detectability of gravitational wave events by spherical resonant-mass antennas

Gregory M. Harry,* Thomas R. Stevenson,† and Ho Jung Paik‡
Department of Physics, University of Maryland, College Park, Maryland 20742
(Received 13 February 1996)

We report on results of computer simulations of spherical resonant-mass gravitational wave antennas interacting with high-frequency radiation from astronomical sources. The antennas were simulated with three-mode inductive transducers placed on the faces of a truncated icosahedron. Overall, the spheres were modeled with a sensitivity of about three times the standard quantum limit. The gravitational radiation data used was generated by three-dimensional numerical computer models of inspiraling and coalescing binary neutron stars and of the dynamical bar-mode instability of a rapidly rotating star. We calculated energy signal-to-noise ratios for aluminum spheres of different sizes cooled to 50 mK. We find that by using technology that could be available in the next several years, spherical antennas can detect coalescing binaries out to slightly over 15 Mpc, the lower limit on the distance required for one event per year. For the rapidly rotating star, we find, for a particular choice of the radius at centrifugal hangup, spheres are sensitive out to about 2 Mpc. The event rate is estimated to be about 1 every 10 years at this distance. [S0556-2821(96)04916-8]

PACS number(s): 04.80.Nn, 04.30.Db, 95.55.Ym

I. INTRODUCTION

The experimental effort to directly detect the space-time ripples known as gravitational waves has been going on for 35 years, beginning with Weber's pioneering work in the early 1960's [1]. Since then, two main experimental approaches have evolved: cryogenic resonant-mass detectors [2–4] and laser interferometers [5–7]. The sensitivity of both techniques is sufficient so that unambiguous detection of gravitational waves is expected soon, perhaps within the next ten years. The work of Taylor and Hulse [8], showing the orbital decay of binary pulsar PSR 1913-16 is in agreement with general relativity's prediction for gravitational wave emission, has added to the anticipation of the first direct, confirmed detection. It appears possible that a new generation of advanced resonant-mass detectors could operate concurrently with interferometers already under construction. At this time, understanding possible sources of gravitational waves and which experimental technique is best suited to which source of radiation takes on greater importance. We endeavor to clarify this by numerically computing energy signal-to-noise ratios for resonant-mass detectors and interferometers interacting with two possible sources of gravitational waves.

The best understood source of detectable gravitational waves is from inspiraling and coalescing binary neutron stars [9]. The Laser Interferometer Gravitational-Wave Observatory (LIGO) has been designed and optimized to detect these events at a distance of 200 Mpc after significant interferometer improvements [5]. To accomplish this, it has been devised to be most sensitive at as low a frequency as possible ($\sim$200 Hz) where the waveform from binary neutron stars is stronger. However, the waveform at 200 Hz is due almost solely to the *inspiral* phase of the binary neutron star evolution and contains virtually no information about the *coalescence*. As the inspiral is determined by point-mass dynamics, the equation of state for nuclear matter (i.e., neutron stars) will affect only the coalescence waveform. Coalescence also occurs when the gravitational field between the neutron stars is strongest, so the effects of general relativity will be more important than during the inspiral. To measure these effects, it will be necessary to monitor the *higher-frequency* waves from coalescence in addition to those at lower frequency from inspiral.

Resonant-mass gravitational wave detectors have been in use for longer than the interferometric detectors. Resonant-mass antennas with bar geometries have been taking data and been continually improved since their inception. The use of spherical geometry as an improvement over bars was first

*Electronic address: gharry@wam.umd.edu
†Electronic address: ts88@umail.umd.edu
‡Electronic address: hp1@umail.umd.edu

suggested by Forward in 1971 [10], and Wagoner and Paik later showed that at equal frequencies spheres have an advantage over bars in energy cross section [11]. Recent reexamination of spherical detectors [12–15] has generated international interest in constructing one or more massive spherical antennas incorporating advances in transducer technology. The possibility of building such an antenna to operate concurrently with the first LIGO interferometers appears good [16]. The sensitive frequencies for a sphere are higher than those for the first LIGO interferometers, spanning about 750 Hz to 2700 Hz in the lowest mode, and therefore they are well suited to complement interferometer experiments at high frequencies. One such advanced resonant-mass detector can be more sensitive than the first LIGO interferometers within a bandwidth of around 100 Hz centered at the quadrupole resonance of the sphere and would have a sensitivity within that band comparable to what will be achieved by the advanced LIGO interferometers. The sphere's sensitivity is independent of source direction, unlike LIGO. Spherical antennas can also provide direction and polarization information more easily than LIGO [13] and, properly instrumented, could detect any scalar gravitational radiation that might be present [10,11]. In this paper, when we refer to ''high-frequency'' gravitational radiation, we mean those signals that include significant strength above 750 Hz. This frequency is where the first LIGO interferometers' sensitivity begins to weaken from photon shot noise in the lasers [5] and the spherical resonant-mass detector's sensitivity becomes important.

We have looked at the question of whether a spherical detector, or in particular a truncated icosahedral gravitational-wave antenna (TIGA) as described by Merkowitz and Johnson [14], is capable of observing high-frequency events. Specifically, the coalescence of a binary neutron star system and the dynamical bar-mode instability of a single, rapidly rotating star were examined as possible astronomical phenomena that could produce high-frequency gravitational radiation. Waveforms for these events, generated with computer simulations by Centrella's group at Drexel University, were used as input into a mathematical model of a 50 mK spherical detector with three-mode inductive transducers [17]. The energy signal-to-noise ratios obtained from this model help determine how TIGA's and interferometer experiments can best complement one another.

Coccia and Fafone [18] have also looked at energy signal-to-noise ratios from astronomical events in spherical detectors. Our work and theirs are complementary. They looked solely at inspiraling binary neutron stars as sources, leaving out the coalescence phase as well as any other high-frequency events. Since the inspiral can be modeled accurately by point-mass dynamics, they used an analytical expression for the waveform. We found it necessary to use numerical data from computer models to simulate the coalescence. By limiting themselves to the inspiral phase, Coccia and Fafone were unable to accurately predict energy signal-to-noise ratios for higher mass neutron stars or black holes. For some sphere sizes and compositions their simulation does not produce results for $1.4M_{\odot}$ neutron stars, the observed mass for all known neutron stars in binaries [9]. However, their method was able to show that spherical antennas can determine the chirp mass $[M_c \equiv (M_1 M_2)^{3/5}/(M_1+M_2)^{1/5}$ [19]], the orbital inclination and the distance to the source, a result our method did not produce. Both techniques provide useful information that are unobtainable by the other.

In Sec. II, we describe the method used for the energy signal-to-noise ratio calculations, how the code that produced the results was written, and what parameters for the spherical antenna we used. In Sec. III, we discuss the signal waveforms we used as inputs into the model developed in Sec. II and present the results of the calculations. Finally, in Sec. IV, we present our conclusions and discuss ideas for further work.

II. METHOD

To calculate the energy signal-to-noise ratio (SNR) per unit bandwidth of the TIGA, we followed the method of Price [20] who showed how to calculate the SNR for a bar antenna that uses an optimal filter to process the data. Stevenson [21] has shown that for six identical transducers in the TIGA geometry and identical Q's for all five quadrupole modes of the sphere, the SNR of a spherical antenna is identical to that of a bar antenna instrumented with one of those six transducers. The *equivalent bar* has an effective mass as seen by the transducer of

$$m_{\rm eff} = \tfrac{5}{6}\chi(\tfrac{4}{3}\pi R^3)\rho, \tag{1}$$

where R and ρ are the sphere radius and density. The dimensionless parameter χ comes from the radial driving point admittance matrix of the sphere at the quadrupole frequency. For an aluminum sphere with a Poisson ratio of 0.33, $\chi = 0.301$ [13]. The factor of 5/6 in Eq. (1) accounts for the multiple sphere modes and transducers [21]. The SNR for the TIGA is the same as that for the equivalent bar provided one equates the energies deposited by the gravitational wave in the two antennas. We can now calculate the SNR for the simpler case of a bar, while retaining all the information available from a sphere.

The energy deposited in the sphere is calculated from

$$E = \mathcal{F}_{\omega}\Sigma, \tag{2}$$

where Σ is the energy cross section of the sphere [13],

$$\Sigma = \frac{G}{c^3}\frac{\rho V_s^5}{f_0^3}\Pi. \tag{3}$$

Here V_s is the extensional sound speed of the sphere material, f_0 is the quadrupole frequency, and Π is a dimensionless constant that accounts for antenna geometry and mode. It has the value 0.215 [13] for a sphere in the lowest quadrupole mode and 0.585 in the first excited quadrupole mode [13,15]. Throughout G and c are Newton's gravitational constant and the speed of light. The total energy flux $\mathcal{F}_{\omega}$ is [22]

$$\mathcal{F}_{\omega} = \frac{c^3}{G}\frac{1}{16\pi}\omega^2|h(\omega)|^2, \tag{4}$$

where ω is the angular frequency of the gravitational radiation and $|h(\omega)|$ is the magnitude of the frequency-domain

amplitude of the gravitational wave. Thus the total energy deposited in the equivalent bar is

$$E=\frac{\pi}{2}\frac{\rho V_s^5}{f_0}\Pi|h(\omega_0)|^2. \tag{5}$$

We define an *effective force* that acts on the equivalent bar [13]:

$$f_{\rm eff}(\omega)=-m_{\rm eff}\omega^2 h(\omega) l_{\rm eff}, \tag{6}$$

where the relationship between $l_{\rm eff}$ and R is determined as follows. For an impulsive force, the energy is deposited as kinetic energy in the antenna. The energy E after the impulse is given by

$$E=\frac{|f_{\rm eff}(\omega_0)|^2}{2m_{\rm eff}}. \tag{7}$$

Combining Eqs. (5)–(7) gives

$$l_{\rm eff}=\sqrt{\Pi\frac{2\pi^2\rho V_s^5}{m_{\rm eff}\omega_0^5}}. \tag{8}$$

Then using Eq. (1) and the relationship between ω_0, V_s, and R [23] for each quadrupole mode an $l_{\rm eff}$ of $0.337R$ in the lowest quadrupole mode and $0.109R$ in the first excited quadrupole mode are calculated. Using Eq. (6) as the definition of a force on the equivalent bar, the method of Price can be followed exactly.

The transducer we assumed was a three-mode inductive transducer. A three-mode transducer is necessary, rather than the standard two-mode system, to get higher bandwidths, which are required to reach sensitivities near the standard quantum limit. Higher bandwidth reduces the requirement on the Q of the sphere and transducer. Higher bandwidth is also useful to cover a larger spectrum of frequencies and reduce the need for additional antennas.

Assuming that a template of the gravitational waveform is available, optimal filtering can be used on the output signal of the transducer. The optimal filter produces the highest SNR possible [24] and has the form

$$K(\omega)=\frac{e^{-j\omega t_0}u^*(\omega)}{S_n(\omega)}, \tag{9}$$

where $u(\omega)$ is the velocity signal of the antenna effective mass and $S_n(\omega)$ is the total velocity noise spectral density, both referred to the input of the optimal filter. The parameter t_0 is the time at which the SNR is to be optimized. To calculate $u(\omega)$ and $S_n(\omega)$, it is necessary to solve the equations of motion for the antenna coupled to the three-mode resonant transducer. They have the form

$$\begin{aligned} j\omega m_{\rm eff}u_1&=f_1-\frac{jk_{\rm int}}{\omega}(u_{\rm int}-u_1)+\frac{jk_{\rm eff}}{\omega}u_1,\\ j\omega m_{\rm int}u_{\rm int}&=\frac{jk_{\rm int}}{\omega}(u_{\rm int}-u_1)-\frac{jk_{\rm trans}}{\omega}(u_2-u_{\rm int})-f_2,\\ j\omega m_{\rm trans}u_2&=\frac{jk_{\rm trans}}{\omega}(u_2-u_{\rm int})+f_2. \end{aligned} \tag{10}$$

Here, $m_{\rm eff}$ is the effective mass of the antenna, $m_{\rm int}$ is the mass of the intermediate resonator, and $m_{\rm trans}$ is the transducer mass; $k_{\rm eff}$ is the effective spring constant of the antenna, $k_{\rm int}$ is the spring constant that connects the antenna to the intermediate mass, and $k_{\rm trans}$ is the spring constant between the intermediate mass and the transducer mass. The spring constants are complex valued and include dissipation. The variables $u_1, u_{\rm int}$, and u_2 are, respectively, the velocities of the antenna surface at the transducer, of the intermediate mass, and of the transducer mass. Applied forces acting on the antenna surface and between $m_{\rm trans}$ and $m_{\rm int}$ are denoted by f_1 and f_2, respectively.

Eliminating $u_{\rm int}$ from Eq. (10) allows the equations of motion to be written as

$$u_i=y_{ij}f_j, \tag{11}$$

with i and j taking the values 1 to 2. The energy SNR per unit bandwidth, $\sigma(\omega)$, then becomes [20]

$$\sigma(\omega)=K(\omega)u_2 \tag{12}$$

$$=\frac{|u_2(\omega)|^2}{S_n(\omega)}. \tag{13}$$

From Eq. (11), $\sigma(\omega)$ is found to be

$$\sigma(\omega)=\frac{|f_1 y_{21}|^2}{S_u+S_f|y_{22}|^2+2k_BT{\rm Re}(y_{22})+2{\rm Re}(y_{22}S_{fu})}, \tag{14}$$

assuming no force on the transducer, i.e., $f_2=0$. Here the force f_1 is $f_{\rm eff}$ from Eq. (6) and T is the physical temperature of the sphere. The matrix $y_{ij}(\omega)$ is the admittance matrix of the antenna with transducer defined in Eq. (11). The four terms in the denominator are the individual parts of $S_n(\omega)$, the velocity noise. They are, respectively, the additive velocity noise, the force noise, the thermal noise, and the correlation noise. The spectral densities are defined as

$$\begin{aligned} S_f(\omega)&\equiv\int_{-\infty}^{+\infty}e^{-j\omega\tau}\langle f(t)f(t-\tau)\rangle d\tau,\\ S_u(\omega)&\equiv\int_{-\infty}^{+\infty}e^{-j\omega\tau}\langle u(t)u(t-\tau)\rangle d\tau,\\ S_{fu}(\omega)&\equiv\int_{-\infty}^{+\infty}e^{-j\omega\tau}\langle f(t)u(t-\tau)\rangle d\tau. \end{aligned} \tag{15}$$

In practice, these noise terms are found not to vary much with frequency in the antenna's sensitive range. It is often convenient to parametrize these spectral densities with three values; noise temperature T_n, noise resistance r_n, and noise reactance x_n. They are defined as

$$T_n=\frac{1}{k_B}\sqrt{S_f S_u-[{\rm Im}(S_{fu})]^2}, \tag{16}$$

$$r_n = \sqrt{\frac{S_f}{S_u} - \left(\frac{\mathrm{Im}(S_{fu})}{S_u}\right)^2}, \tag{17}$$

$$x_n = \frac{\mathrm{Im}(S_{fu})}{S_u}, \tag{18}$$

where k_B is Boltzmann's constant. For simplicity, we set $\mathrm{Im}(S_{fu})=0$. Although, in general, the correlation between the force and velocity noise is nonzero, the effects of a nonzero S_{fu} can normally be accounted for by a renormalization of the transducer spring constant [20]. The real part of S_{fu} is normally zero when a superconducting quantum interference device (SQUID) amplifier is used.

Once a complete expression for $\sigma(\omega)$ has been obtained, the energy SNR can be calculated from

$$S/N = \frac{1}{2\pi}\int_{-\infty}^{+\infty} \sigma(\omega)\, d\omega. \tag{19}$$

Note that we have consistently used a double-sided spectral density in contrast to the single-sided convention adopted by LIGO. By putting in numerical values for all parameters, this integral can be evaluated. For many of the parameters below, we chose values beyond what has been demonstrated experimentally so as to represent an advanced spherical detector. Such an advanced detector could operate concurrently with the first LIGO interferometer as a result of aggressive research and development efforts now being planned [16]. Some of our parameter values are only slight extrapolations beyond currently demonstrated values, while others are instead upper bounds to the technologies being pursued. A detailed consideration of the research burden to meet each of our assumed values is beyond the scope of this paper. As stated in the introduction, our motivation is to clarify how such spherical detectors could complement the interferometer experiments by examining the detectability of high frequency events. We feel it is likely that resonant-mass detectors with an energy sensitivity approaching that derived with our parameters can be developed and built to operate within the time frame between the completion of the first LIGO interferometers and the operation of advanced interferometers.

We chose to model aluminum spheres at a physical temperature of 50 mK, instrumented with six identical sets of three-mode inductive transducer systems located with the dodecahedral TIGA geometry [14]. The lowest temperature that an aluminum bar antenna has been successfully cooled to is 95 mK [25]. Two-mode transducers are in use on a number of operating cylindrical resonant-mass antennas [2–4] and a three-mode system has been demonstrated at 4 K in a smaller, test antenna [26]. A constant mass ratio between the effective mass of the sphere and the intermediate mass as well as between the intermediate and transducer masses of 100:1 was used, and all mechanical quality factors (Q's) were assumed to be 40×10^6. The highest mechanical Q that has been obtained in an inductive transducer is 24×10^6 [27].

The transducer electronics were assumed to be a 9 cm diameter inductive pickup coil attached to a SQUID amplifier with a quantum-limited noise temperature, i.e., $T_s = 1\hbar\omega_0/k_B$. Quantum-limited SQUID's have been constructed [28], but they are not useful for inductive transducers because of their low input coil inductance. Getting a suitable quantum-limited SQUID is an area of intense research. Wellstood's group at the University of Maryland is developing a quantum-limited SQUID for use in a gravitational wave transducer. The best noise temperature they have achieved in a SQUID with high enough inductance to couple to the transducer coils is $T_s \approx 28\hbar\omega_0/k_B$ [29]. The prospect of approaching the quantum-limit in a practical SQUID in the next several years looks real. With proper matching, the transducer noise is limited by the noise of the SQUID, so the value of T_n in Eq. (16) becomes equal to T_s. The noise resistance is $r_n = k_E/4\pi f_0$, where k_E is the real part of the spring constant k_{trans} that is due to the electrical interaction between the transducer mass and the pickup coils. The ratio k_E/k_{trans} is the coupling between the electrical and mechanical parts of the transducer. For the value k_E, we took the product 3.78×10^8 N/m$^3\times$ coil area, based on measurements made in our laboratory at Maryland [30].

Taken together, these parameters define the overall sensitivity of the antenna. Energy sensitivity E_s is defined as

$$E_s = \frac{E}{S/N}. \tag{20}$$

It is useful to express this sensitivity in relation to the standard quantum limit, the minimum sensitivity possible using a linear amplifier [31]. Expressed as a multiple of this standard quantum limit, the antenna sensitivity becomes

$$N = \frac{E_s}{\hbar\omega_0}. \tag{21}$$

As a comparison for the numerical result, we calculate an approximate value of N from

$$N \approx \frac{k_B}{\hbar\omega_0}\left[T_s + \frac{T}{\delta}\left(\frac{1}{\alpha_1 Q_{\mathrm{eff}}} + \frac{1}{\alpha_2 Q_{\mathrm{int}}} + \frac{1}{\alpha_3 Q_{\mathrm{trans}}}\right)\right]. \tag{22}$$

Equation (22) is derived in the Appendix. The parameters δ and α_i are also defined and computed in the Appendix. Substituting the values of T, T_s, Q_{eff}, Q_{int}, and Q_{trans} assumed above into Eq. (22) gives

$$N \approx 1.0 + 0.96 + 0.87 + 0.78 \approx 3.6. \tag{23}$$

We calculated SNR's for eight different spheres. The diameter of the lowest-frequency sphere was chosen to be the largest size that might be constructed, 3.25 m. The size of the highest-frequency sphere was chosen so that its lowest quadrupole frequency coincides with the peak in the spectrum of the coalescing binary neutron star data. This peak is at twice the rotation frequency of the transient, barlike structure that forms immediately after coalescence [32]. This assumption gives a sphere diameter of about 1.05 m. The remaining sphere sizes were chosen to give reasonably continuous coverage of the frequency band 750 Hz to 2700 Hz. In addition to transducers tuned to the lowest quadrupole mode of the sphere, a system tuned to the first excited mode was examined. Coccia, Lobo, and Ortega [15] have shown that the cross section of the excited mode of a large sphere is 2.72 times greater than that for the lowest mode of a small sphere

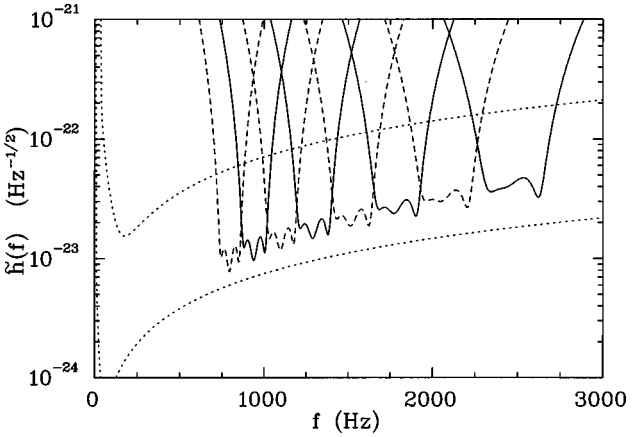

FIG. 1. The strain spectrum of the eight spherical antennas in the lowest quadrupole mode, shown with solid and dashed lines. The different line styles have no significance other than to differentiate the separate strain spectra. The upper dotted line shows the strain spectrum for the first LIGO interferometer and the lower dotted line shows the strain spectrum for the advanced LIGO interferometer, for reference. The spherical antennas, each with a sensitivty about 3 times the standard quantum limit, are more sensitive than the first LIGO interferometers in a bandwidth of about 100 to 300 Hz each and together span a total bandwidth from 750 to 2700 Hz. In this band, the spherical antennas are a little less sensitive than the advanced LIGO interferometers.

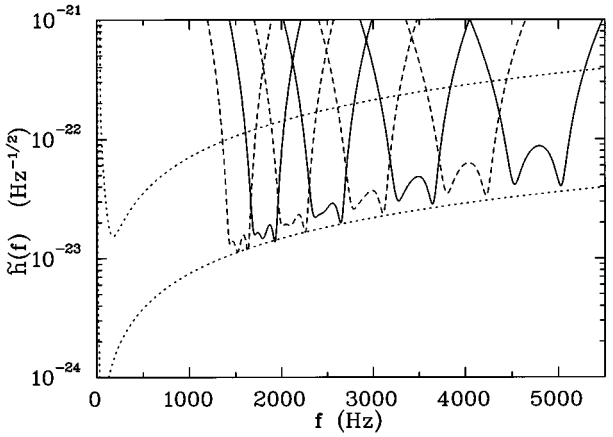

FIG. 2. The strain spectrum of the eight spherical antennas in the first excited quadrupole mode, shown with solid and dashed lines. The different line styles have no significance other than to differentiate the separate strain spectra. The upper dotted line shows the strain spectrum for the first LIGO interferometer and the lower dotted line shows the strain spectrum for the advanced LIGO interferometer, for reference. The spherical antennas, each with a sensitivity about 3 times the standard quantum limit, are more sensitive than the first LIGO interferometers in a bandwidth of about 200 to 600 Hz each and together span a total bandwidth from 1350 to 5100 Hz. In this band, the spherical antennas are about equal to the sensitivity of the advanced LIGO interferometers.

at the same resonance frequency. This allows the calculations of SNR's for the higher mode.

Figures 1 and 2 show the sensitivities of the eight spheres in the ground state and excited state, respectively. These figures also show the sensitivity of the first LIGO and advanced LIGO interferometers for comparison. The data graphed is the *strain spectrum* of the detectors, $\tilde{h}(\omega)$, defined as

$$\tilde{h}(\omega)=\sqrt{\frac{|h(\omega)|^2}{\sigma(\omega)}}. \tag{24}$$

The strain spectrum is a measure of what frequency distribution an incoming gravitational wave would have to have in order to produce an output in a noiseless detector that mimics the output of the real detector's noise. It is a useful way to compare detectors because it is independent of source waveform and thus is solely a characteristic of the antenna. The energy SNR per unit bandwidth, $\sigma(\omega)$, is related to the quantities h_c and $h_{\rm rms}$ used by LIGO as defined in Ref. [5] by

$$\sigma(\omega)=\frac{1}{2f}\left(\frac{h_c}{h_{\rm rms}}\right)^2. \tag{25}$$

Using these quantities, a value for the SNR of LIGO is often estimated as the maximum value of $[h_c/(\sqrt{5}h_{\rm rms})]^2$, which gives a rough approximation to the integral in Eq. (19). The factor of $\sqrt{5}$ is necessary to convert to ''random direction and polarization'' [33].

These figures show that the spherical resonant-mass antennas have a sensitivity intermediate between the first and advanced LIGO interferometers within a fractional bandwidth of about 10% each. The collection of all the TIGA's, or the ''xylophone,'' is a more sensitive detector than the first LIGO interferometers from 750 Hz to 2700 Hz in the lowest mode and from 1350 Hz to 5100 Hz in the first excited mode. In these frequency regions LIGO's sensitivity is constrained by photon shot noise in the lasers [5].

III. SIGNALS AND RESULTS

In order to integrate $\sigma(\omega)$ and obtain the SNR for the spherical antenna, numerical values for a gravitational wave-

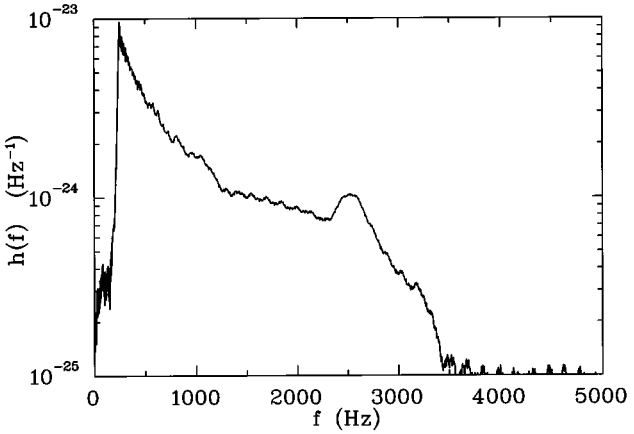

FIG. 3. The frequency-domain gravitational waveform averaged over source orientation from the inspiral and coalescence of two neutron stars with mass $1.4M_\odot$ and radius 10 km at 15 Mpc from the antenna. The sharp cutoff at 300 Hz is due to the finite extent of the time-domain data. The spectrum from 300 to about 1000 Hz is due mainly to the inspiral phase. The frequency $f_{\rm dyn}=1566$ is the dynamical instability frequency. The peak at $f\approx 2500$ Hz is associated with the transient barlike structure that forms immediately following the onset of coalescence [32].

form from an astronomical event are needed. For inspiraling and coalescing binary neutron stars, we used the waveform published by Zhuge, Centrella, and McMillan [32]. We Fourier transformed the time-domain data using the convention $h(\omega)=\int_{-\infty}^{\infty}e^{-j\omega t}h(t)dt$. Although the calculation by Zhuge *et al.* is among the most complete available, it is still only a first survey of how binary neutron stars may behave. In particular, it models gravity with a purely Newtonian formula. The inclusion of general-relativistic corrections may significantly change the orbit and lead to differences in the waveform. Our results derived using this waveform should be seen in this light.

The frequency-domain waveform for the inspiral and coalescence phase of the binary neutron star evolution is shown in Fig. 3. Zhuge *et al.* generated the waveform using a three-dimensional numerical simulation which models the neutron stars as nonrotating polytropes. The neutron stars were chosen to have equal masses of $1.4M_{\odot}$ each, since all known cases of neutron stars in binary systems have this mass [9]. Initially, the distance between the stars was chosen to be much larger than the diameter of individual stars, so tidal gravitational effects are negligible. Thus, the stars are originally spherical, with a radius of 10 km. The initial orbit was chosen to be nearly circular and it evolves due to Newtonian gravity with a frictional term added to simulate the energy loss to gravitational wave emission. When the stars spiral together, tidal distortions in each star's shape grow larger and the evolution approaches coalescence.

Once the separation between the stars is comparable to the neutron star's radius, hydrodynamic effects become important and an approximation of the nuclear equation of state is required. Zhuge *et al.* used

$$P=K\rho^{1+1/n} \tag{26}$$

as the equation of state, where P is pressure, ρ is density, K is a constant that measures the specific entropy of the nuclear matter, and n is the polytropic index. A value of $n=1$ was used for the waveform we analyzed. Smooth particle hydrodynamics (SPH) is then used to model the coalescence phase once the equation of state is specified.

The gravitational waveform was calculated from the complete orbit of the binary neutron star system using the quadrupole approximation by Zhuge *et al.* This approximation ignores contributions from mass moments higher than the quadrupole, but is valid for nearly Newtonian sources [22]. In the transverse-traceless (TT) gauge, the gravitational wave amplitude is

$$h_{ij}^{\mathrm{TT}}=\frac{G}{c^4}\frac{2}{r}\ddot{I}_{ij}^{\mathrm{TT}}, \tag{27}$$

where $\ddot{I}$ is the second time derivative of the reduced quadrupole mass moment of the source. The amplitude of the ''plus'' and ''cross'' polarizations of the gravitational wave, expressed in spherical coordinates, are

$$h_{+}=\frac{G}{c^4}\frac{1}{r}(\ddot{I}_{\theta\theta}-\ddot{I}_{\phi\phi}), \tag{28}$$

TABLE I. Energy signal-to-noise ratios for binary neutron star evolution in the lowest $l=2$ mode of the sphere. The distance to the neutron stars is taken to be 15 Mpc and each neutron star has a mass of $1.4M_{\odot}$ and a radius of 10 km. The waveforms have been averaged over source and detector angles. The individual spheres have a sensitivity about 3 times the standard quantum limit. The row labeled ''xylophone'' is obtained by summing the signal-to-noise ratios for each sphere.

Diameter (m)	Frequency (Hz)	Coalescence	Inspiral	Total
3.25	795	0.0113	10.6	11.3
2.75	940	0.00985	5.79	6.28
2.35	1100	0.0146	3.43	3.88
2.00	1292	0.00948	1.40	1.64
1.70	1520	0.00853	0.907	1.09
1.45	1782	0.0104	0.558	0.719
1.25	2096	0.0197	0.285	0.449
1.05	2461	0.126	0.0886	0.407
Xylophone		0.210	22.8	25.6
First LIGO interferometers		0.00406	58.2	58.8

$$h_{\times}=\frac{G}{c^4}\frac{2}{r}\ddot{I}_{\theta\phi}. \tag{29}$$

The absolute scale of these amplitudes requires a choice for r, the distance from the detector to the source. We used $r=15$ Mpc, the approximate distance to the Virgo cluster of galaxies [33]. This distance is estimated by Phinney [9] to be below the most optimistic value to get 3 events per year, 23 Mpc. Scaling from this value, about 1 event per year is predicted at 15 Mpc in this optimistic limit.

The waveform from the Newtonian inspiral with friction was then meshed onto the waveform from SPH by Zhuge *et al.* to get a complete waveform for the whole binary neutron star evolution. Since the orientation angles of the binary system are not known *a priori*, and in fact are values that the spherical antenna can determine experimentally [18], we averaged the waveform over these unknown angles. This averaging is done so that the energy per frequency, dE/df, radiated by the binary system is held constant. Thus, in Eq. (5),

$$|h(\omega)|^2=\langle|h_{+}(\omega)|^2+|h_{\times}(\omega)|^2\rangle, \tag{30}$$

where $\langle\cdots\rangle$ denotes an average over all source angles. It is this waveform that is shown in Fig. 3 and was used as input in Eq. (14).

Once a numerical expression for the waveform $h(\omega)$ was made available to us, it was possible to obtain SNR's for the eight spheres with the diameters shown in Table I. To do this, the integral in Eq. (19) must be evaluated. Performing this integration with the $h(\omega)$ from Eq. (30) gave the SNR's in the column marked ''total'' in Table I. The row marked ''xylophone'' is what an array of all eight TIGA's acting together could accomplish and is the sum of each SNR in the rows above. The row marked ''first LIGO interferometers'' is for comparison with the first LIGO interferometers and was calculated by using the same waveform integrated with the strain spectrum published for LIGO [5]. Since the waveform is of finite extent in time, the frequency domain data is

TABLE II. Energy signal-to-noise ratios for binary neutron star evolution in the first excited $l=2$ mode of the sphere. The waveforms have been averaged over source and detector angles. The distance to the neutron stars is taken to be 15 Mpc and each neutron star has a mass of $1.4M_{\odot}$ and a radius of 10 km. The individual spheres have a sensitivity about 3 times the standard quantum limit. The row labeled ''xylophone'' is obtained by summing the signal-to-noise ratios for each sphere.

Diameter (m)	Frequency (Hz)	Coalescence	Inspiral	Total
3.25	1528	0.0235	2.43	2.93
2.75	1806	0.0289	1.45	1.88
2.35	2113	0.0593	0.679	1.13
2.00	2483	0.349	0.222	1.09
1.70	2921	0.0688	0.0448	0.224
1.45	3425	0.00709	0.00591	0.0252
1.25	3973	0.00111	0.00150	0.00513
1.05	4729	0.000674	0.000733	0.00279
Xylophone		0.538	4.83	7.29
First LIGO interferometers		0.00406	58.2	58.8

not accurate below 300 Hz. In order to get a reasonable value for the SNR of LIGO, it was necessary to extrapolate the data below this cut off and into LIGO's sensitive region. We did this with the analytical waveform in Eq. (44) of Ref. [33]. Note that this equation as published has a factor of 2 error. The value $\pi/12$ should be instead $\pi/6$ [34]. We used the corrected version for the extrapolation. It was also necessary to divide the LIGO SNR by a factor of 5 to represent a wave with random direction and polarization [33]. This correction is unnecessary for the spherical antennas because they are equally sensitive in all directions.

To determine how effective the TIGA's can be in observing the coalescence phase of the binary neutron star evolution, we separated the waveform into two parts. The inspiral occurs from $t=0$ s to $t=0.234$ s, and the coalescence occurs from $t=0.234$ s to $t=0.241$ s. This division of time was chosen so that the instantaneous frequency at $t=0.234$ s coincides with $f_{\rm dyn}$, the dynamical instability frequency identified by Zhuge *et al.* as the frequency where the neutron stars cease to act as point masses. The separate time-domain waveforms were then multiplied by a Hahn windowing function [35] before Fourier transforming, to ensure that the division was smooth and no spurious high-frequency signals were artificially created. The SNR's obtained from each of these separate waveforms are shown in the columns marked ''inspiral'' and ''coalescence,'' respectively, in Table I.

With the results, we can calculate the energy sensitivity E_s achieved by the spheres from Eq. (20). The energy deposited in the 3.25 m sphere in the lowest mode is 1.79×10^{-29} J, from Eq. (5). Thus, with a SNR of 11.3,

$$E_s=\frac{1.79\times10^{-29}\ \mathrm{J}}{11.3}=3.0\hbar\omega_0, \tag{31}$$

in good agreement with the approximate calculation in Eq. (22).

We also calculated SNR's for the spheres instrumented with resonant-mass transducers tuned to the first excited mode of the antenna. The same physical parameters were used to model the spheres and the same waveforms used as signals. This data is shown in Table II.

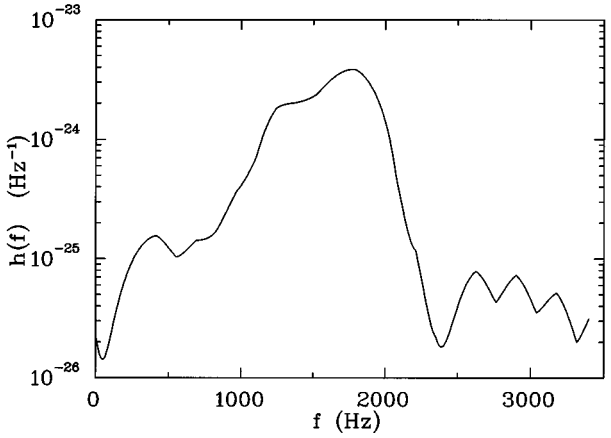

FIG. 4. The frequency-domain gravitational waveform averaged over source orientation from the bar-mode instability of a rapidly rotating star of mass $1.4M_{\odot}$ and radius at centrifugal hangup of 20 km at a distance of 1 Mpc from the antenna. The primary peak at 1765 Hz is twice the rotational frequency of the star.

Binary neutron star events are the best understood signals for gravitational wave detection, but because of the high operating frequency of spherical antennas, other astronomical sources may be important for the spheres. One possible high-frequency signal is from the dynamical bar-mode instability of a rapidly rotating star. This event may be detectable by spherical antennas provided the star is compact enough. The stellar radius that this event occurs at is uncertain. This instability has been investigated by Smith, Houser, and Centrella [36] and it is their numerical waveform data that we used.

Figure 4 shows the spectrum for the bar-mode instability which develops following ''centrifugal hangup'' during the core collapse of a massive star. This gravitational waveform was generated by Smith *et al.* using three-dimensional numerical simulations which modeled the star as a polytrope, with equation of state

$$P=\frac{\rho\epsilon}{n}. \tag{32}$$

Here P is pressure, ρ is density, ϵ is specific internal energy, and n is the polytropic index. A value of $n=3/2$ was used for the waveform in our simulation. A total mass of $1.4M_{\odot}$ was assumed, as the star is expected to end up as a neutron star. An equatorial radius for the centrifugal hangup of 20 km was also assumed. This is the radius where the star's collapse is arrested by the centrifugal effects from the rotation. A realistic value for this radius is not known, but could range from as high as 3000 km down to as low as 10 km [37]. The initial rotation had a ratio of rotational kinetic energy to gravitational potential energy of $\tau\approx0.30$. Newtonian gravity was assumed and the gravitational radiation produced from the dynamical bar-mode instability was calculated in the quadrupole approximation, as with the coalescence waveform. Back reaction from gravitational wave emission was ignored. The bar mode, i.e., $m=2$ mode, was used as it is expected to

TABLE III. Energy signal-to-noise ratios for the rapidly rotating star waveform for $l=2$ modes of the sphere. The waveforms have been averaged over source and detector angles. The dashes for the excited mode of the 1.45, 1.25, and 1.05 m spheres represent the fact that the signal data cuts off below the resonance frequency of these modes. The distance to the star is taken to be 1 Mpc, the mass of the star is taken to be $1.4M_{\odot}$, and the radius of centrifugal hangup is taken to be 20 km. The individual spheres have a sensitivity about 3 times the standard quantum limit. The row labeled ''xylophone'' is obtained by summing the signal-to-noise ratios for each sphere.

	Ground state		Excited state	
Diameter (m)	Frequency (Hz)	SNR	Frequency (Hz)	SNR
3.25	795	0.0661	1528	19.5
2.75	940	0.220	1806	25.0
2.35	1100	1.22	2113	1.08
2.00	1292	4.75	2483	0.00434
1.70	1520	6.95	2921	0.00278
1.45	1782	9.91	3425	-
1.25	2096	0.935	3973	-
1.05	2461	0.00168	4729	-
Xylophone		24.1		45.6
First LIGO interferometers		0.197		0.197

be the fastest growing mode [36]. This waveform was generated for the *dynamical* bar instability, which is driven by Newtonian hydrodynamics and gravity rather than the *secular* instability, which is due to dissipative processes such as gravitational radiation reaction. The dynamical instability develops on a time scale of about one rotation period while the secular instability grows over several periods or even more slowly. The choice of $\tau=0.30$ is just above the dynamical stability limit of 0.2738 [38] and thus is a reasonable approximation for a star that spins up, due to collapse or accretion, and becomes dynamically unstable [36]. The star's evolution was simulated by Smith *et al.* using SPH and from this evolution the gravitational waveform is calculated by using Eq. (27).

The choice of r, the distance from source to detector, is not as simple as for the binary neutron star. There is less observational evidence for stars with bar-mode instabilities. Such rapidly rotating stars may be formed from supernovae, so the rate of supernovae might be taken as a reasonable guide to the rate of this gravitational wave event. Out to the Virgo cluster of galaxies (15 Mpc), the supernovae rate is estimated at a few per year [39]. We took the source distance to be $r=1$ Mpc, which has an estimated event rate of 1 every 10 years [39]. Once the magnitude of each polarization state was evaluated, the same average over angles as in Eq. (30) was performed to give the waveform shown in Fig. 4. The SNR's were calculated by using the method described in Sec. II. These values are shown in Table III for both the ground state and the first excited quadrupole modes. The 1.45 m, 1.25 m, and 1.05 m diameter spheres do not have data listed for the excited mode because the frequency-domain waveform cuts off at 3500 Hz, which is below the resonance frequencies of these spheres. This is because the granularity of the time domain data provided was too great for frequencies above 3500 Hz. However, we believe it is safe to assume that the frequency-domain data would remain below $h(\omega)=10^{-25}$ Hz^{-1} and thus the SNR's for these three spheres would be negligible.

The secular instability can develop for τ values greater than 0.1375 [38]. After the dynamical instability has run its course, Houser *et al.* find the system has evolved to a nearly axisymmetric state with a core having $\tau=0.26$, which is above the secular instability limit. Lai and Shapiro [38] have investigated the secular instability which may develop in which a Maclaurin spheroid evolves into a Dedekind ellipsoid producing a gravitational wave signal sweeping in frequency from possibly near 1 kHz down to zero. A different type of secular evolution would apply if the calculations of Durisen *et al.* [40] or Williams and Tohline [41] correctly predict the end point of the dynamical instability as a bar surrounded by a ring, rather than the spheroid found by Houser *et al.* If a rapidly spinning bar is produced, the secular evolution changes the bar from a Jacobi-like ellipsoid into a Maclaurin spheroid with a gravitational wave signal from 500 Hz to as high as 3 kHz.

Lai and Shapiro give analytical waveforms for these two different secular instabilities. For the same $1.4M_{\odot}$ star at 1 Mpc with a radius of 10 km averaged over all source and detector angles, the Dedekind waveform would give an energy SNR of 2000 in the 3.25 m diameter sphere and 1200 for the first LIGO interferometers. Such a strong signal would be detectable even at the Virgo cluster distance. However, it seems likely that the starting frequency for the Dedekind evolution will be well below the spherical detector's band unless the star is initially spinning just below the dynamical instability limit and is nearly incompressible. In order for the starting frequency of this event to exceed the 795 Hz frequency of the 3.25 m sphere, Lai and Shapiro's Fig. (5) indicates one needs a polytropic index $n<0.7$ for $\tau=0.26$, while even $n=0$ does not suffice for $\tau\leqslant 0.24$. In contrast, the frequency span of the signal from Jacobi-like evolution seems to have a higher possibility of overlap with the band covered by the spheres; however, the chief uncertainty for that signal is whether or not the dynamical instability produces a spinning bar rather than a spheroid. *If* Jacobi-like evolution occurs and its starting frequency is below 800 Hz, then the signal computed by Lai and Shapiro is a very strong source for a big sphere: we calculate an energy SNR of 4000 for a 3.25 m diameter sphere and an energy SNR of 240 for the first LIGO interferometers from a waveform averaged over all angles and a source distance of 1 Mpc.

IV. CONCLUSION

The results in Table I for the spherical antenna tuned to the lowest quadrupole frequency interacting with gravitational radiation from binary neutron stars shows that spherical antennas operate at a level that is complementary with the first LIGO interferometers. The largest sphere obtains an energy SNR of 11.3 at a distance of 15 Mpc. If a SNR of 10 in this detector is a sufficient threshold for a three-way coincidence experiment, then a source with angle averaged strength could be detected out to a distance of 15.9 Mpc. With the most optimistic estimate of the coalescence rate, 3

events per year out to 23 Mpc [9], the expected rate of detection r_d is

$$r_d = 1.15 \times 3 \ \ \mathrm{yr}^{-1} \left(\frac{15.9 \ \ \mathrm{Mpc}}{23 \ \ \mathrm{Mpc}} \right)^3 \tag{33}$$

$$= 1.15 \ \ \mathrm{yr}^{-1}. \tag{34}$$

The factor of 1.15 is due to statistical preference for angles that give high SNR's (see [33] for details). For detection of gravitational radiation from binary neutron stars at a distance of 15 Mpc, a 3.25 m diameter aluminum sphere near the standard quantum limit will be sufficient. The upper limit on the event rate at this distance is about 1 coalescence per year [9].

Table I also shows that a large sphere instrumented at the lowest quadrupole frequency does not hold out much hope of seeing the details of binary neutron star coalescence. Even the 1.05 m diameter sphere, whose size was chosen so that the lowest quadrupole mode was at the maximum of the coalescence wave spectrum, does not manage to reach a SNR of 1. As the frequency of the sphere goes up, the radius, and with it its mass, goes down. At frequencies where the waveform from Zhuge *et al.* is strong, the energy cross section of the sphere is too small to detect much. This raises the question of the reliability of the numerical waveform, especially of the frequency f_{peak} associated with the barlike transient. According to Centrella [42], the qualitative shape of the waveform is fairly reliable, but the exact position of this peak and other structures may change as numerical relativity techniques improve. If f_{peak} were to be found at a lower frequency, closer to the lowest quadrupole mode of one of the larger spheres, the prospect for a SNR greater than 1 for the coalescence phase might improve.

The data in Table II for spheres sensitive at the first excited quadrupole mode to inspiraling and coalescing binary neutron stars appears a little more promising for the detection of coalescence. The largest sphere still has the highest overall SNR, but it is reduced from its value in the ground state. The 2.00 m diameter sphere, with an excited quadrupole frequency of 2483 Hz, is now the sphere tuned to f_{peak}. It does not quite manage a SNR of 1 either, but it does have a higher SNR for the coalescence than for the inspiral phase, as do the 1.70 m and 1.45 m spheres.

The data in Tables I and II, taken together, suggest that a xylophone of spheres acting collectively and in collaboration with LIGO may be the best approach to detection of binary neutron star coalescence. The smaller spheres do not contribute much to the xylophone SNR, so four spheres, from 3.25 m to 2.00 m in diameter, would be enough to give most of the xylophone benefits. If these four spheres could be instrumented at both the ground and the first excited quadrupole frequencies, a fairly wide spectrum, from 750 Hz to 2700 Hz continuously, could be monitored. The spheres could rely on LIGO to provide a high SNR detection of the inspiral. Once the event is discovered, the spheres would have the less strenuous task of identifying and analyzing the high frequency coalescence. Thus, even the modest SNR's found in our work may still prove useful in gathering astrophysical data on coalescing binary neutron stars.

The data for the rapidly rotating star shown in Table III is more encouraging. For the ground state modes, the 1.45 m sphere has its frequency near the peak of the spectrum and obtains a strong SNR of almost 10. The two spheres with quadrupole frequencies below the resonance of the 1.45 m sphere also have strong SNR's, about 7 and 5. Further away from the peak, SNR's fall off rapidly, especially on the high-frequency end. The SNR goes from 0.935 for a sphere diameter of 1.25 m to well below 1 for a diameter of 1.05 m. Thus with only two antennas the peak signal can be easily found, provided their sensitive frequencies occur at the appropriate positions.

The first excited state data is similar to the ground state, showing strong SNR's when the sphere's quadrupole frequency is at or near the 1765 Hz peak. In the excited mode, however, this occurs between the 3.25 m and the 2.75 m diameter spheres. With larger masses, these spheres have higher energy cross sections and thus obtain much higher SNR's. A SNR of 25, from the 2.75 m sphere in the excited state, represents such a strong signal that the source position on the sky could be located to within almost 0.13 steradian [13]. As with the ground state data, there is a sharp drop in SNR to effectively zero about 500 Hz above the peak frequency, making location of the peak frequency possible.

The rapidly rotating star waveform was generated by assuming a total mass of $1.4 M_{\odot}$ and a centrifugal hangup at 20 km. The location of the peak frequency, which is twice the rotation frequency of the star, is very sensitive to the values of these parameters. It can be as low as 1 Hz for a $1.0 M_{\odot}$, 3000 km star up to 6000 Hz for a $2.0 M_{\odot}$, 10 km star [37]. Since the appropriate values for these star parameters are not known, and in fact are values we could hope to determine from gravitational wave data, actual signals from this source could potentially be outside the sensitive range of spherical antennas. A peak frequency above about 2500 Hz, corresponding to a $1.4 M_{\odot}$, 10 km star, would be extremely difficult to detect outside our galaxy. This would limit the number of events to a few per century. Detecting these higher frequency signals depends on the accuracy of the current template, especially the secondary peak in Fig. 4 at 400 Hz. Many details of the rapidly rotating star's evolution are not well understood and this waveform may undergo substantial changes as the field of numerical relativity advances.

A xylophone of a 3.25, 2.75, 2.35, and a 2.00 m diameter sphere instrumented at both the ground state and the first excited quadrupole state working along with LIGO, as suggested for the inspiraling and coalescing binary neutron stars, would do an effective job of searching for rapidly rotating star events. For favorable mass and radius parameters, the excited state of the 2.75 m diameter sphere would be sensitive, with a SNR threshold of 10, out to 1.6 Mpc. This will be sufficient to observe one event every decade, provided nearly all type $\mathrm{I_b}$ and type II supernovae are sources of this event [39]. This xylophone would also determine the star's rotation frequency, as a large SNR would be seen in the more massive sphere and effectively nothing would be seen in the smaller. This would locate the peak frequency, and hence the rotation frequency, to within a few hundred hertz. Negative results from such a xylophone would restrict the parameter space, providing data about neutron star development and equation of state. The xylophone covers a fre-

quency range corresponding to hangup radii between 45 km down to 15 km. The broadband interferometers have difficulty detecting this dynamical instability, but do have a high SNR for the secular instability. Since these two gravitational wave events may occur in succession, a collaborative effort between spheres and interferometers would prove effective as with the binary neutron stars.

In this paper, we have compared broadband interferometers with resonant-mass antennas for detection of high frequency gravitational radiation. Another possible technique for detecting high frequency events involves dual-recycled interferometers [43]. This approach allows laser interferometers to become much more sensitive within a narrow bandwidth at the expense of sensitivity elsewhere. Krolak, Lobo, and Meers [43] have looked at SNR's for inspiraling neutron stars interacting with recycled interferometers using a simplified strain spectrum and an analytical formula for the waveform. Their results for the unrecycled LIGO are in close agreement with ours. Further investigations of SNR's comparing spherical antennas with dual-recycled interferometers is being done at Caltech [34].

In addition to the astronomical sources of gravitational radiation that we investigated here, there may be other high frequency signals potentially detectable in detectors optimized for the 1–2 kHz band. Events that might produce high-frequency gravitational waves include coalescence of a neutron star with a black hole or a black hole with a second black hole [19], asymmetric core collapse and bounce in supernovae [19], spinning neutron stars [44], and cosmic string vibrations [45]. Especially promising may be the black hole coalescences and spinning neutron stars. Excitation of the high-frequency [$f \approx 1200-3250$ Hz $(10M_{\odot}/M)$ [46]] black hole quasinormal modes would give a relatively strong signal at kilohertz frequencies. A gravitational-wave antenna detection of this radiation could provide the observational ''smoking gun'' to confirm the existence of black holes. Experimental evidence of gravitational radiation from black hole coalescence would undoubtedly also provide great insight into relativistic gravity. Spinning neutron stars are a periodic source that could radiate strongly for months [44]. The frequency of the waves would be twice the rotation period, often above a kilohertz, and details of the wave would tell much about the structure of neutron stars. According to Thorne, [19] ''the deepest searches for these nearly periodic waves will be performed by narrow-band detectors . . . , e.g., dual recycled interferometers or resonant-mass antennas.'' We call on the numerical relativity community to continue to develop reliable waveforms for all possible high-frequency events. It is only through the combined efforts of everyone, interferometer and resonant-mass experimentalists, as well as numerical and analytical theorists, that confirmed, direct detection of gravitational radiation will become a reality.

ACKNOWLEDGMENTS

We would like to thank J. M. Centrella and J. L. Houser for providing us with the numerical data for their gravitational waveforms. We also thank J. M. Centrella, J. L. Houser, S. A. Hughes, C. W. Misner, J.-P. Richard, S. R. Sinha, K. S. Thorne, F. W. Wellstood, and X. Zhuge for helpful discussions as well as R. K. Burrows and P. C. Dulany for invaluable computer assistance and comments. This work was supported by NSF Grant No. PHY93-12229.

APPENDIX: ASYMPTOTIC EXPANSION OF THE ENERGY SENSITIVITY

Equation (20) defines the energy sensitivity E_s as the ratio of E, the energy the signal would deposit in a bare antenna initially at rest, to the SNR calculated by integrating $\sigma(\omega)$ given by Eq. (14). Although we calculated E_s directly in this fashion, useful insight into the dependence of E_s on the detector parameters comes from considering the asymptotic behavior for the Q_i approaching infinity as indicated by Eq. (22).

First, consider the lossless case when all Q's are infinite. Then $\mathrm{Re}(y_{22})$ is zero, and Price [20] shows that the expression for $\sigma(\omega)$ can be rewritten exactly as

$$\sigma(\omega) = \frac{e_n(\omega)}{k_B T_n}, \tag{A1}$$

where

$$e_n(\omega) = \frac{|f_1 y_{21}|^2}{|1 + z_n y_{22}|^2} r_n, \tag{A2}$$

T_n is the mechanical amplifier noise temperature defined by Eq. (16), and

$$z_n = r_n + j x_n \tag{A3}$$

is the mechanical amplifier's complex noise impedance, defined by Eqs. (17) and (18).

As Price [20] explains, $e_n(\omega)$ has the following physical interpretation: it is the spectrum of the energy which would be dissipated in r_n if the signal were applied when the amplifier had been replaced by its input impedance plus an additional mechanical impedance equal to z_n. If $f_1(\omega)$ varies little over the band where $e_n(\omega)$ is large, then the signal is approximately an impulsive force which deposits the energy

$$E = \frac{|f_1(\omega_0)|^2}{2m_{\mathrm{eff}}} \tag{A4}$$

initially all in antenna motion. Since the hypothetical detector with z_n inserted is assumed lossless except for r_n, eventually 100% of the energy E ends up being dissipated in r_n. Thus from this physical argument we have

$$\int_{-\infty}^{\infty} \frac{d\omega}{2\pi} e_n(\omega) \approx \frac{|f_1(\omega_0)|^2}{2m_{\mathrm{eff}}}, \tag{A5}$$

independent of the values of r_n and the detector masses and springs. Therefore, in the lossless case, the SNR is

$$S/N=\int_{-\infty}^{\infty}\frac{d\omega}{2\pi}\sigma(\omega) \tag{A6}$$

$$=\int_{-\infty}^{\infty}\frac{d\omega}{2\pi}\frac{e_n(\omega)}{k_BT_n} \tag{A7}$$

$$\approx\frac{E}{k_BT_n}, \tag{A8}$$

provided f_1 and T_n vary little over the frequencies where e_n is significant. Hence, for an impulsive force, $E_s=k_BT_n$ in the lossless case independent of the other detector parameters.

Next, consider the case where all Q's are infinite except that for the antenna. Then the antenna dissipation produces a thermal force noise acting on $m_{\rm eff}$ with spectral density $2k_BTm_{\rm eff}\omega_0/Q_{\rm eff}$. Therefore, Eq. (14) becomes

$$\sigma(\omega)=\frac{|f_1y_{21}|^2}{S_u+S_f|y_{22}|^2+2\mathrm{Re}(y_{22}S_{fu})+2k_BT(m_{\rm eff}\omega_0/Q_{\rm eff})|y_{21}|^2}. \tag{A9}$$

For convenience, we define the energy sensitivity expressed in temperature units to be T_p, the detector's pulse-detection noise temperature:

$$k_BT_p=E_s. \tag{A10}$$

Motivated by Eq. (26) in Price [20], we use Eqs. (A1) and (A2) to rewrite Eq. (A9) in terms of $e_n(\omega)$, and then expand the integral for SNR to first order in $Q_{\rm eff}^{-1}$ and use Eq. (A5):

$$S/N=\frac{E}{k_BT_p} \tag{A11}$$

$$=\int_{-\infty}^{\infty}\frac{d\omega}{2\pi}\frac{e_n(\omega)}{k_BT_n}\frac{1}{1+(T\omega_0/T_nQ_{\rm eff})[e_n(\omega)/E]} \tag{A12}$$

$$\approx\frac{E}{k_BT_n}\left(1-\frac{T\omega_0}{T_nQ_{\rm eff}2\,\delta f_0}\right), \tag{A13}$$

where

$$2\,\delta f_0=\frac{[\int_{-\infty}^{\infty}(d\omega/2\pi)e_n(\omega)]^2}{\int_{-\infty}^{\infty}(d\omega/2\pi)[e_n(\omega)]^2} \tag{A14}$$

defines the fractional bandwidth δ of the lossless detector in a way which arises naturally in the SNR expansion, and which agrees with the intuitive definition of bandwidth if $e_n(\omega)$ is box shaped.

Thus when all other Q's are infinite, the asymptotic form of E_s for large $Q_{\rm eff}$ is described by

TABLE IV. Coefficients in the asymptotic expansion of energy sensitivity. The α_i determine the influence of the Q's on the noise temperature. The value δ is the fractional bandwidth of the detector in the lossless limit.

Constant	Calculated	Theoretical
α_1	0.34	$1/\pi = 0.32$
α_2	0.41	-
α_3	0.40	-
δ	0.103	$\sqrt{m_{\rm trans}/m_{\rm int}}=0.100$

$$\frac{1}{T_p}\approx\frac{1}{T_n}\left(1-\frac{T\omega_0}{T_nQ_{\rm eff}2\,\delta f_0}\right), \tag{A15}$$

$$T_p\approx T_n+\frac{T}{Q_{\rm eff}\delta}\pi\ \text{ as }\ Q_{\rm eff}\longrightarrow\infty. \tag{A16}$$

When other Q's besides $Q_{\rm eff}$ are also finite, analysis along the lines above is more cumbersome, but one finds

$$T_p\approx T_n+\frac{T}{\delta}\sum_{i=1}^{N}\frac{1}{\alpha_iQ_i}, \tag{A17}$$

where the constants α_i can be determined numerically. Comparison with Eq. (A16) shows that $\alpha_1=1/\pi$ always. Thus, a higher fractional bandwidth δ reduces the effect of finite Q's on T_p.

Price [20] argues that a clever choice of the masses and springs to maximize δ for a given value of r_n is the optimal design strategy, and that a design in which $e_n(\omega)$ is made ''optimally flat'' is nearly optimal in this sense. However, in this paper, we have chosen the simpler design originally proposed by Richard [47] which has constant successive mass ratios since we find both designs give similar values for T_p.

The values of α_i for $i\geqslant 2$ depend on the masses and springs chosen for the detector design. The values for α_1, α_2, and α_3 that we calculated and used are shown in Table IV. These values are for the case of a constant mass ratio between stages of 100. This ratio was chosen as a convenient value that gives a final transducer mass slightly higher than the mass that gives the lowest T_p. A higher mass is more resistant to uncertainties in noise resistance and thus is preferred experimentally to a lower than optimal mass. The design rule suggested by Richard [47] for choosing a constant mass ratio given an r_n and $m_{\rm eff}$ can be written as

$$\left(\frac{m_{i+1}}{m_i}\right)^{(2N-1)/2}=\zeta\frac{r_n}{m_{\rm eff}\omega_0}, \tag{A18}$$

where N is the number of modes of the system and ζ is 2. The design we chose corresponds to $N=3$ and $\zeta=2.61$; the α_i in Table IV apply for any such design.

[1] J. Weber, Phys. Rev. **117,** 306 (1960).
[2] W. W. Johnson *et al.*, in *Gravitational Wave Experiments*, Proceedings of the First Edoardo Amaldi Conference, Frascati, Italy, edited by E. Coccia, G. Pizzella, and F. Ronga (World Scientific, Singapore, 1995).
[3] F. Ricci *et al.*, in *Gravitational Wave Experiments* [2].
[4] M. E. Tobar *et al.*, in *Gravitational Wave Experiments* [2].
[5] A. Abramovici *et al.*, Science **256**, 325 (1992).
[6] C. Bradaschia *et al.*, Nucl. Instrum. Methods Phys. Res. A **289**, 518 (1990).
[7] K. Danzmann *et al.*, in *Relativistic Gravity Research*, Proceedings of the 81 WE-Heraus-Seminar, Bad Hannef, Germany, edited by J. Ehlers and G. Schäfer (Springer-Verlag, Berlin, 1992).
[8] J. H. Taylor, Rev. Mod. Phys. **66**, 711 (1994); R. A. Hulse, *ibid.* **66**, 699 (1994).
[9] E. S. Phinney, Astrophys. J. **380**, L17 (1991).
[10] R. L. Forward, Phys. Rev. D **2**, 149 (1971).
[11] R. V. Wagoner and H. J. Paik, in *Experimental Gravitation*, Proceedings of the Pavia International Symposium, Pavia, Italy (Academia Nazionale dei Lincei, Rome, Italy, 1977).
[12] W. W. Johnson and S. M. Merkowitz, Phys. Rev. Lett. **70**, 2367 (1993).
[13] C. Z. Zhou and P. F. Michelson, Phys. Rev. D **51**, 2517 (1995).
[14] S. M. Merkowitz and W. W. Johnson, Phys. Rev. D **51**, 2546 (1995).
[15] E. Coccia, J. A. Lobo, and J. A. Ortega, Phys. Rev. D **52**, 3735 (1995).
[16] An American collaboration among researchers at the University of Maryland, Louisiana State University, the University of Rochester, and the University of Santa Clara has been formed to design and build spherical antennas. There are also collaborations in Italy, the Netherlands, and Brazil.
[17] H. J. Paik, J. Appl. Phys. **47**, 1168 (1976).
[18] E. Coccia and V. Fafone, Phys. Lett. A (to be published).
[19] K. S. Thorne, in *Proceedings of the Snowmass 95 Summer Study on Particle and Nuclear Astrophysics and Cosmology*, edited by E. W. Kolb and R. Peccei (World Scientific, Singapore, in press).
[20] J. C. Price, Phys. Rev. D **36**, 3555 (1987).
[21] T. R. Stevenson, in *Gravitational Wave Experiments* [2].
[22] C. W. Misner, K. S. Thorne, and J. A. Wheeler, *Gravitation* (Freeman, New York, 1973).
[23] A. E. H. Love, *A Treatise on the Mathematical Theory of Elasticity* (Dover, New York, 1944).
[24] L. A. Wainstein and V. D. Zubakov, *Extraction of Signals from Noise* (Prentice-Hill, Englewood Cliffs, NJ, 1962), Chap. 3.
[25] E. Coccia *et al.*, in *Gravitational Wave Experiments* [2].
[26] W. M. Folkner, Ph.D. thesis, University of Maryland, 1987.
[27] Z. Geng, Ph.D. thesis, Louisiana State University, 1994.
[28] D. D. Awschalom *et al.*, Phys. Rev. Lett. **62**, 199 (1989); M. W. Cromar and P. Carelli, Appl. Phys. Lett. **38**, 723 (1981); D. J. Van Harlingen, R. H. Koch, and J. Clarke, Physica B **108**, 1083 (1981).
[29] F. W. Wellstood (private communication).
[30] The MATHEMATICA code used to generate our results is available on the World Wide Web at http://www.physics.umd.edu/rgroups/gen_rel_exp/snr.html.
[31] R. P. Giffard, Phys. Rev. D **14**, 2478 (1976).
[32] X. Zhuge, J. M. Centrella, and S. L. W. McMillan, Phys. Rev. D **50**, 6247 (1994).
[33] K. S. Thorne, in *Three Hundred Years of Gravitation*, edited by S. W. Hawking and W. Israel (Cambridge University Press, Cambridge, England, 1987).
[34] K. S. Thorne (private communication).
[35] C. D. McGillem and G. R. Cooper, *Continuous and Discrete Signal and System Analysis* (Holt, Rinehard and Winston, New York, 1974).
[36] S. C. Smith, J. L. Houser, and J. M. Centrella, Astrophys. J. **458**, 236 (1996).
[37] J. L. Houser (private communication).
[38] D. Lai and S. L. Shapiro, Astrophys. J. **442**, 259 (1995).
[39] S. van den Bergh and G. A. Tammann, Annu. Rev. Astron. Astrophys. **29**, 363 (1991).
[40] R. H. Durisen *et al.*, Astrophys. J. **305**, 281 (1986).
[41] H. A. Williams and J. E. Tohline, Astrophys. J. **334**, 449 (1988).
[42] J. M. Centrella (private communication).
[43] A. Krolak, J. A. Lobo, and B. J. Meers, Phys. Rev. D **43**, 2470 (1991).
[44] M. Zimmermann and E. Szedenits, Phys. Rev. D **20**, 351 (1979).
[45] A. Vilenkin, in *Three Hundred Years of Gravitation* [33].
[46] F. Echeverria, Phys. Rev. D **40**, 3194 (1989).
[47] J.-P. Richard, in *Proceedings of the Second Marcel Grossmann Meeting on General Relativity*, Trieste, 1979, edited by R. Ruffini (North-Holland, Amsterdam, 1982); Phys. Rev. Lett. **52**, 165 (1984).